

Tailoring transport in quantum spin chains via disorder and collisions

Vittoria Stanzione, Alessandro Civolani,^{*} Maria Luisa Chiofalo,[†] and Jorge Yago Malo
Physics Department and INFN, Pisa University, Pisa, I-56127, Italy .

(Dated: March 10, 2025)

We systematically investigate the interplay of disorder and space-time heterogeneous collisional noise in shaping the transport dynamics of an anisotropic XXZ spin chain. Using stochastic collision models to simulate interaction with the environment, we explore the localization-delocalization transitions across regimes with single and multiple excitations. We find that space homogeneous collisions occurring at low rates favor the shaping of regions where the localization degree sets in the form of subsequent plateaus at a rate and duration universally scaling with the collision rate. We also find that interactions among the excitations favor this process even for tiniest levels of disorder.

Our findings can be applied to design stroboscopic protocols where sequences of transport and localization can be tailored. We establish relevant connections to noise-engineering of quantum devices in noisy intermediate-scale quantum simulators platforms, and to realistic biological systems where noise and disorder coexist.

I. INTRODUCTION

Quantum transport governs charge, spin and energy transfer in a wide variety of systems, from solid-state physics and spintronics to quantum technologies [1–4]. In fact, by exploring the effects of disorder, noise, and interactions, we can gain insights into the mechanisms driving localization-delocalization transitions, thermalization, and the emergence of collective phenomena in low-dimensional and complex systems. In particular, current technologies enable the study of quantum transport with the engineering of reduced-dimensionality systems in solid state and in AMO (atomic, molecular, and optical) platforms [5, 6].

Paradigmatic many-body Hamiltonians in open quantum networks are important models as they represent essential functions and can be engineered in tunable current experiments used as quantum simulators [7]. We are interested in biology applications [8, 9] and on coarse-grained models within the so-called quantum-like paradigm [10, 11]. In general, regardless of the presence of quantum effects in the performance of specific biological processes, the statistics of quantum mechanics and the open quantum system framework [12–15] provides us with a well-suited mathematical toolbox to describe complex phenomena, both quantum and classical, into potentially simpler and representative models [11, 16].

Quantum effects in biological systems present a fascinating yet debated area of research, challenging conventional views on the role of quantum mechanics in the warm and noisy environment of living organisms. These physics-based models can incorporate quantum effects into the description of microscopic phenomena allowing us to study how a noisy and out-of-equilibrium biological environment is influenced by coherent and dissipative quantum effects [8, 17, 18].

In general, the behavior of transport in a quantum system serves as a powerful diagnostic tool for understanding thermalization in disordered conditions [19]. In the absence of interactions, disorder can induce Anderson localization [20], where transport is suppressed due to interference effects, preventing the system from reaching thermal equilibrium. Interactions or noise disrupts this localization mechanism, leading to a transition toward diffusive or even ballistic transport, depending on the system's parameters [21, 22]. The transition from localized to delocalized regimes provides insight into how thermalization emerges in complex systems. Consequently, disorder is a mechanism that suppresses transport in isolated systems and, in open systems, also a factor that competes with noise to dictate the system's relaxation dynamics.

In [16], we explored how dissipation modulates transport in an open quantum system using stochastic collision models accounting for space and time heterogeneous collisions. In so doing, we could focus on the interplay between noise, interactions, and coherence under sufficiently general conditions. By tuning noise parameters, we demonstrated controllable modifications to transport properties, identifying regimes where increasing the collision rate enhances transport. Thus, we showed that engineered dissipation can counteract localization effects.

We now focus on the combination of collisional noise and disorder which provides a model that closely mirrors the dynamics of transport in many complex media including those relevant to biological systems. Collisional models replicate approximate interactions with noisy warm environment, while disorder introduces local spatial inhomogeneities. Together, these elements capture key features of energy transfer in systems where coherent and dissipative processes coexist relevant in several fields of physics, like charging and discharging performances in open quantum system batteries [23, 24], transport in an engineered environment of complex systems [25] along with many body localization in 1-D systems [26]. Moreover, the tunability of collisional noise parameters enables the simulation of biologically relevant scenarios, such as the exploitation of noise-assisted trans-

^{*} Physics Department and SUPA, Strathclyde University, Glasgow G4 0NQ, UK

[†] corresponding author: marilu.chiofalo@unipi.it

port [27, 28].

In this paper, we investigate the transport properties and thermalization dynamics of a noisy, disordered XXZ spin chain [29–32], modeled through stochastic collision processes. Among different possibilities, we adopt this many-body model for its capability of describing in a general manner tunneling-based transport of excitations in the presence of coherent anisotropic interactions. We identify localization/delocalization transitions and thus transport windows for multiple excitations tuning the interplay of disorder, anisotropy, and noise.

The paper is organized as follows. In Section II we present the model of our disordered spin-chain interacting with the environment via stochastic collision models and introduce the figures of merit adopted to study transport properties. In Section III, we present the results of our study comparing the cases of one, two and multiple injected excitations also highlighting the entanglement properties in those regimes. Finally, in Section IV we present our conclusions and discuss future perspectives in the light of technological progress in quantum science and biology.

II. MODEL AND METHODS

The conceptual model setting is sketched in Fig. 1 (a). We investigate an integrable generalization of the Heisenberg spin chain that accounts for uni-axial anisotropy [33] with the addition of a disorder term:

$$H_{XXZ} = J \sum_{i=1}^{N-1} [\sigma_i^x \sigma_{i+1}^x + \sigma_i^y \sigma_{i+1}^y + \Delta \sigma_i^z \sigma_{i+1}^z] + h \sum_{i=1}^N r_v(1, i) \sigma_i^z, \quad (1)$$

and subjected to dissipation through noise in the form of stochastic collision models, as depicted in Sec. II A, with open boundary conditions (OBC). In Eq. 1, $\sigma_i^{x/y/z}$ are the Pauli operators acting on spin located at site i ; J is the spin exchange rate, that can also be seen as the tunneling amplitude for excitation quasiparticles throughout the system; Δ governs the anisotropy in the form of a spin-spin interaction along the z-axis. In our analysis, we consider the regime with $J = 1 (> 0)$ and then scale every other energy to J . As a result, the ground state with disorder $h = 0$ is a ferromagnet for $\Delta > 1$, becoming a critical paramagnet for $\Delta \leq 1$. The introduction of disorder in the form of a random local field proportional to σ_i^z with amplitude h breaks the integrability of the model. Thus, different ground states would occur under different disorder realizations. The disorder for every spin is then randomly generated, according to the random vector $r_v(max, i)$ varying between (0,1) for each site independently, in each individual simulation for every site in a range $[-h, h]$.

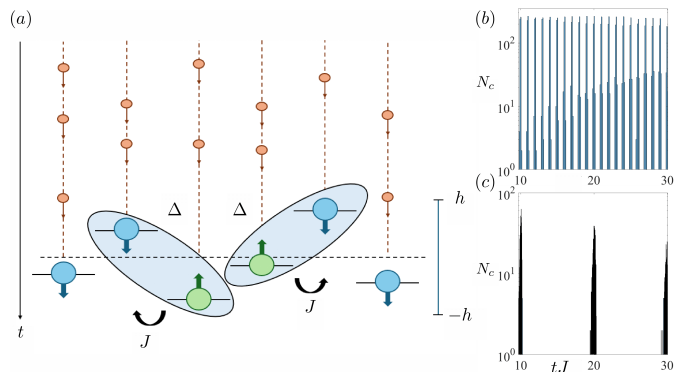


FIG. 1. Sketch of our model. (a) Open quantum spin chain with energy levels affected by disorder in the $[-h, h]$ range. Excitations are depicted as flipped spins (green), their dynamics being affected by the tunneling rate J (black arrows), interaction strength Δ (blue ovals) and the addition of a noisy environment. This is represented by the auxiliary light-brown qubits colliding with the sites over time. (b)-(c) Histograms displaying the number of collisions undergone by the auxiliary qubits (log scale) against our spins over time tJ for a noise shape parameter of $\nu = 100$ in the time-uniform regime, and collision rates $r_c = 1$ (b) and (c) $r_c = 0.1$. We use the same simulation parameter: number of sites in the spin is $N = 41$ sites, $M = 500$ trajectories and final time of simulation $tJ = 30$.

When considering the time evolution of excitations or quench dynamics, the disorder term will control different transport regimes, ranging from ballistic to diffusive, and it can lead to the emergence of Many-Body localization (MBL) [34]. In fact, disorder can lead to the breakdown of thermalization, meaning that the system fails to reach thermal equilibrium at long times resulting in transport suppression. Tuning the disorder through h and analyzing the resulting transport behavior, it is possible to map the parameter regimes where localization or delocalization dominates.

A. Noise modeling

So far we have discussed how the coherent and disorder-driven terms of our model are described. Here, we introduce dissipation through a particular discretization of the environment degrees of freedom (d.o.f.) that lies in the family of stochastic collision models [9, 35]. This type of environment description comprises heterogeneous interactions in time and space with a bath composed of a set of itinerant d.o.f. This modeling represents an effective approximation to what happens in a biological system [9, 36]. As depicted in Fig.1, the environment d.o.f are modeled as auxiliary qubits (light brown circles) that collide over time with the spins in the chain.

In this approach, we can govern the noise regimes via appropriate distributions describing the probability of system-environment interaction events. This results

into a flexible environment description, including non-trivial temporal correlations even remaining within a Markovian-like description. As it is the case for many dissipative dynamical maps, stochastic collisional models are compatible with many local quantum channels. In our case, we account for density-density collisions decorrelating spins from the coherent evolution, thus effectively producing dephasing in the system degree of freedom.

We choose to describe the collisional rate between spins and auxiliary d.o.f. by adopting the especially flexible Weibull distribution [9, 37]:

$$p(t) = \frac{\nu}{\mu} \left(\frac{t}{\mu} \right)^{\nu-1} e^{-(t/\mu)^\nu}, \quad (2)$$

where indeed the shape parameter $\nu \geq 0$ controls the time heterogeneity structure, and the scale parameter $\mu > 0$ governs its overall rate. Specifically, collisions are heterogeneous over time for $\nu \leq 1$ and homogeneous for $\nu \gg 1$ while the intercollision time becomes constant. In contrast, the scale parameter is related to the overall collision rate that we define below:

$$r_c = \frac{1}{\tau_{th}} = \frac{1}{\mu \Gamma(1 + 1/\nu)}, \quad (3)$$

with τ_{th} being the mean collision time and Γ given by $\int_0^t \tau p(\tau) d\tau = \Gamma(1 + 1/\nu)$ from Eq. (2). In Fig. 1.(b)-(c), we present histograms for the number of collisions as a function of time for homogeneous noise ($\nu = 100$) and two different collision rates modifying how recurrent is the interaction with the environment.

When collisions occur according to the probability distribution, a quantum channel is applied [9, 38]. This is given by:

$$\Phi[\rho(t_i)] = \text{Tr}[U_{\text{coll}}(\rho_a \otimes \rho(t_i))U_{\text{coll}}^\dagger], \quad (4)$$

with $U_{\text{coll}} = \exp[-i(\pi/2)\sigma_a^x \otimes \sigma_i^z]$ representing the collision event and t_i being the time before the given collision. For a detailed description, we refer to our previous work [16].

Consequently, three competing mechanisms act on the spin chain: coherent coupling between spins, local disorder, and noise originating from the Weibull distribution.

B. Characterizing transport

Having described our model, we now introduce the figures of merit that we use to characterize the system transport and quantify the magnetization spreading (delocalization behavior of the excitations). For one excitation, we use the inverse participation ratio (IPR), $\text{IPR} = \sum_{i=1}^N \langle i | \rho(t) | i \rangle^2$, where i represents the site index and $|i\rangle$ represents the single-excitation localized states

$\{|i\rangle : |i\rangle = \sigma_i^\dagger |0\rangle^{\otimes N}\}$ [9]. The IPR is a measure of localization, bounded between the complete delocalization asymptotic value $\text{IPR} = 1/N$, and $\text{IPR} = 1$, corresponding to complete localization, i.e. when the excitation remains on a particular site of the network [39]. The larger the IPR, the more localized the excitation is over the lattice.

Instead, for a generic number of excitations we use the *Inverse Ergodicity Ratio* (IER) $\text{IER}(t) = \sum_j \langle j | \rho(t) | j \rangle$, defined in terms of the multiple-excitation states $|j\rangle$ that compose our computational basis [16]. IER has the following asymptotic behaviours: $\text{IER} = 1/\dim\mathcal{H}$ implies that the system is in a superposition of all the possible states in the reduced magnetization sector basis, thus the state is *ergodic* [40]; $\text{IER} = 1$, instead, refers to the case in which the system is in one out of these specific configurations, that forms part of our basis. For more details on these two figures of merit in a similar context, we refer to [16].

Our system is a disordered spin-chain, thus we expect a competition between disorder (h), coherent tunneling (J), anisotropy (Δ), and noise (r_c, ν) that could provide a rich landscape where localization and delocalization transitions can be explored.

Therefore, to characterize the emergence of parameter regions where the system (de)localizes, we also consider the behaviour of the entanglement entropy for selected scenarios. The entanglement entropy constitutes one of the well-known heralds of MBL [21, 41], as it presents logarithmic growth in many body localized systems. While not generally accessible in experiments with a few important exceptions [42, 43], the study of entanglement entropy in thermal and non-thermal many-body states [44] has helped understand and quantify the degree of correlation and information spreading between system parts, whereas its behaviour can become non-trivial in regions close to the transition point [45]. The entanglement entropy can be characterized via the Von Neumann entropy [46] defined as follows: consider a bi-partite system composed by A and B subsystems, then the entanglement entropy is $S_{vN} = -\rho_A \log \rho_A$, with $\rho_A = \text{Tr}_B \rho$ the reduced density matrix of subsystem A . Since we are interested in regions in which transport can be modulated to occur only in well-defined time windows, we analyze the behaviour of entanglement entropy as a complementary figure of merit.

III. RESULTS

A. One excitation case

We begin by building our intuition on the interplay between disorder and noise with the case of one single excitation propagating through the disordered spin chain. In this analysis we highlight the fundamental differences between Anderson localization [21] and noise-induced trans-

port. Anderson localization, driven exclusively by disorder, is characterized by the suppression of transport due to interference effects in the absence of any environmental interactions. In contrast, transport induced by collisional noise introduces a competing mechanism, where dephasing disrupts localization and promotes delocalization over time. By focusing on the one excitation case, we simplify the system dynamics, isolating the interplay between disorder and noise while avoiding complications arising from multiple excitation interactions.

We summarize in Fig. 2 the IPR behavior. Fig. 2(a) summarizes the long-time behavior of the Inverse Participation Ratio (IPR) at time $tJ = 30$ as a function of the shape parameter ν and the collision rate r_c . We see that for low values of r_c , the system exhibits higher localization (larger IPR). This occurs because the low collision rate allows for transient localization before delocalization takes place due to noise. More frequent collisions (larger r_c) disrupt these localized states and drive the system toward delocalization, with the IPR approaching its asymptotic value $1/N$. To see the competing effect of disorder, we show in Fig. 2(b)-(c) the IPR evolution at fixed shape parameter $\nu = 100$ in the regime of time-homogeneous collisions. The IPR time evolution is displayed in Fig. 2(b) for various collision rates r_c and fixed large disorder range $h = 10$. We then show in Fig. 2(c) the IPR versus time for different disorder range constants h from 0.1 to 10 at fixed low collision rate $r_c = 0.1$. We observe that low collision rates ($r_c < 1$) and high levels of disorder ($h \gg 1$) lead to transient localization, as evidenced by the formation of sharp plateaus in the IPR. These interesting plateau features reflect moments of temporary stabilization in the system's dynamics, after which collisions induce delocalization. Conversely, at higher collision rates ($r_c \geq 1$), the increased frequency of noise events prevents significant localization, driving the system toward a diffusive regime. Here, the IPR evolves smoothly over time without plateaus formation. The case of $\Delta \neq 0$ was not reported here because the inclusion of an anisotropic interaction term is seen to not qualitatively alter the system's behavior in the single-excitation regime. For more details see [16].

All in all, we observe that noise generally leads to delocalization even in the presence of disorder for any collision rate $r_c \neq 0$. This behavior occurs because the noise-induced dephasing leads to progressive heating of the system, ultimately driving it toward a high-entropy $T = \infty$ steady state with the excitation uniformly distributed across all sites. Disorder slows down the process by creating localized regions that act as traps and inhibits transport by delaying the redistribution of energy. Consequently, while the system eventually reaches the $T = \infty$ state regardless of the disorder strength, the time required to do so increases with higher levels of disorder. This highlights the competing roles of noise, which promotes delocalization, and disorder, which instead favors localization.

In the case of collisions that are homogeneous in time

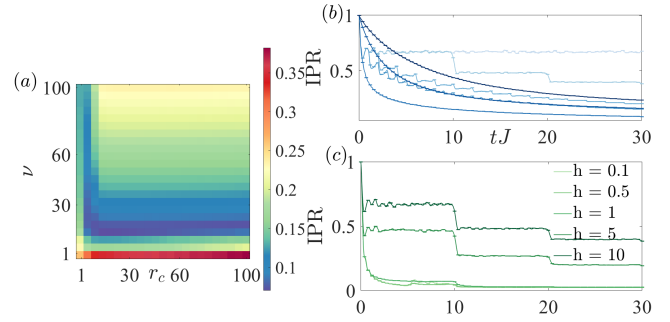


FIG. 2. (De)localization behaviour: one excitation case. Inverse Participation Ratio (IPR) for a spin chain with $N = 41$ sites. (a) IPR at long time ($tJ = 30$), for $h = 10$ and different shape parameters ν and collision rates r_c . (b) IPR vs time for large disorder range $h = 10$ for different collision rates r_c . Curves with progressively increasing tickness and color scale refer to increasing values of $r_c = 0, 0.1, 0.5, 1, 5, 50, 100$ (c) IPR vs time tJ for low $r_c = 0.1$ and different disorder range h . Notice the emergence of plateaus of temporary stabilization of localized behavior. For (b) and (c) the shape parameter is $\nu = 100$ in the time-homogeneous collision regime. The data refer to the case of no anisotropy ($\Delta = 0$ in Eq. 1) since they are seen to be not significantly altered by finite $\Delta \neq 0$. The simulations were performed with $M = 500$ trajectories and $dt = 0.02$.

and in space, that is e.g. with $r_c = 0.1$ and $\nu = 100$ in the figure, noise appears in well defined time slots. This makes visible the corresponding moments where magnetization and IPR change, exhibiting formation of plateaus in the IPR. In this case, we highlight that the higher the value of the disorder, the sharper the plateau. Also, we stress that the plateaus were not affected by the anisotropy. For $r_c < 1$, the excitation exhibits localization, which persists until noise is introduced into the system at well-defined times (see Fig. 1(b)). These noise events induce delocalization, after which the excitation becomes localized again until a subsequent collision perturbs the system dynamics. This process repeats iteratively, leading the IPR to eventually approach its asymptotic value $1/N$, i.e. to the appearance of a fully delocalized state.

In contrast, for $r_c \geq 1$, the frequency of collision events becomes sufficiently high to prevent any significant re-localization of the system. This behavior is particularly evident for $r_c = 1$, as shown in Fig. 1(c). For $r_c \geq 1$, the system transitions to a regime dominated by frequent collisions, which suppress the transient localization observed at lower collision rates. In this regime, the IPR evolves smoothly over time without forming plateaus, indicating sustained delocalization. High collision rates prevent the system from stabilizing in a localized state, continuously redistributing the excitation across the chain. The comparison between homogeneous ($\nu \gg 1$) and heterogeneous ($\nu \leq 1$) noise regimes reveals distinct transport behaviors. In fact, for homogeneous noise, collisions occur at regular intervals, leading to predictable dephas-

ing effects and smoother transitions between localization and delocalization. In contrast, heterogeneous noise introduces temporal variability in collisions, resulting in intermittent localization and a more irregular evolution of the IPR. This highlights the role of noise structure in modulating transport dynamics.

B. Multiple excitations

To shape our understanding of the system's dynamics, we analyze the case of multiple excitations. This introduces additional complexity since interactions between the excitations mediated by anisotropy, disorder, and noise, play a critical role in determining the transport and localization behavior. We systematically analyze how these interactions evolve over time and their dependence on the collision rate r_c , the disorder range constant h , the shape parameter ν , and the anisotropy Δ . Before proceeding with this program, following the outcomes of [16], we first analyze how the anisotropy affects the delocalization behavior. This will allow us to identify the most interesting regimes to zoom in. For more than one excitation IPR is no longer suited and, following [16], we resort to the Inverse Ergodicity Ratio (IER).

1. Effect of anisotropy for two excitations

To capture these effects, we consider two distinct initial configurations for just two excitations: adjacent to each other and separated by two spins, respectively.

We show in Fig. 3(a) the time evolution of the IER for two excitations initially injected at a distance of two spins apart in a system of $N = 20$ sites, subjected to collision rates r_c (from 0 to 1) at fixed temporal homogeneity $\nu = 100$, anisotropy $\Delta = 2.5$, and a high disorder range $h = 10$. The general trend indicates that lower collision rates ($r_c \ll 1$) lead to prolonged localization with the IER remaining closer to 1: the system's state is dominated by a limited number of basis configurations. As r_c increases, the IER decreases more rapidly over time, signaling enhanced delocalization due to frequent noise-induced perturbations. For intermediate collision rates $r_c \sim 0.5$, we observe a gradual reduction of the IER, while for higher rates $r_c \geq 1$, the system rapidly approaches ergodic behavior. For completeness, we display in the inset of Fig. 3(a) the magnetization spread at fixed collision rate $r_c = 0.1$, the other parameters being unchanged.

Consistently with the single-excitation scenario, the emergence of plateaus in the IER remains evident in the presence of noise. However, we now see that the plateaus are stabilized by the anisotropy interaction term even for lower disorder (small h values) when the excitations are injected next to each other (see also the difference between Fig. 7(a) and Fig. 7(b) in Appendix B). This sug-

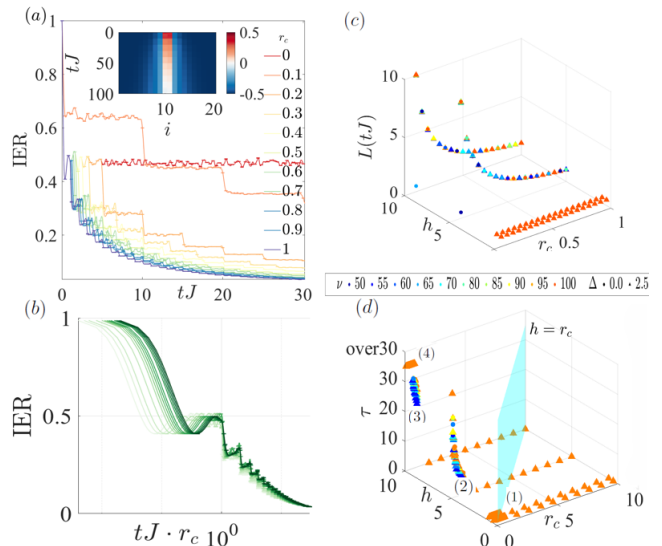


FIG. 3. Effect of anisotropy: the case of two excitations. Inverse Ergodicity ratio (IER) with associated magnetization, plateau length and delocalization time τ for a spin chain of $N = 20$ sites and final time of simulations $tJ = 30$. (a) IER vs time tJ for different collision rates r_c with anisotropy strength $\Delta = 2.5$. Inset: magnetization map over sites i and time tJ , showing the spreading of the two excitations over time. The two neighbouring excitations are initially separated by two spins with very homogeneous collisions over time ($\nu = 100$) and high disorder range with $h = 10$. The IER has the same trend of the IPR and we focus here on the collision rate regime $0 \leq r_c \leq 1$, proved to be more interesting due to the formation of plateaus. For lower collision rates ($r_c \ll 1$) the systems remains localized (IER closer to 1), while increasing r_c leads to a faster delocalization (IER decaying to its limit). (b) IER vs tJr_c varying the collision rate parameter $0 \leq r_c \leq 1$, at fixed high time-homogeneity ($\nu = 100$), high disorder strength ($h = 10$), and in the presence of anisotropy, considering two excitations initially separated by two spins. Curves with progressively increasing thickness refer to values of r_c increasing from 0.20 to 1.00 by 0.05 each. We see that all curves collapse in the region where plateaus are present since they are naturally shifted with respect to each other. (c) 3D plot of plateau length L in terms of tJ vs disorder range $h \in [0, 10]$ and collision rate $r_c \in [0, 1]$. (d) 3D plot of the complete delocalization time τ vs $h \in [0, 10]$ and $r_c \in [0, 10]$. The plane $r_c = h$ separates high τ regions from the small τ ones. In (c) and (d) different colors and shapes for the symbols represent different levels of collision time-homogeneity (colors) and anisotropy (shapes) as in the legend. Also, we show data from two excitations initially injected both next to each other and separated by two spins. The simulations were performed with $M = 250$ trajectories and $dt = 0.02$.

gests that when more excitations are present, anisotropy works to favor the system localization.

In contrast, an increase in the collision rate promotes transport by breaking the pinning of the excitations, an effect facilitated by noise. This can be seen as a manifestation of stochastic resonance, in fact happening also without disorder [16]. In addition, in the case of two

separated excitations at the beginning, the presence of anisotropy doesn't modify the IER behaviour for small values of h .

Consequently, we come to the conclusion that when the two excitations start next to each other and the presence of interaction is significant, the IER behaviour is affected even for weaker disorder. Instead, when they start separated, the impact of their interaction can be considered a sub-leading effect, not significantly affecting the IER. We notice from Fig. 7(a) that for larger collision rates, before the plateaus are well developed, the IER curves at different r_c values tend to collapse, indicating indeed that delocalization gets progressively insensitive to collision events once these become more frequent. It is therefore natural to ask whether a similar universal-type behavior can be identified also in the regime of rare collision events. To this aim, we show the same data in Fig. 7(b) but now with time rescaled with r_c . We indeed see that all curves collapse in the region where plateaus are present. This occurs because the plateau length scales as $1/r_c$ and the different curves are thus naturally shifted with respect to each other.

To have a complete understanding of the plateaus formation, we systematically explored how all the governing system parameters (disorder, time and space homogeneity, and anisotropy) affect the degree of localization. Our findings are summarized in Fig. 3(c)-(d), highlighting an intricate interplay in shaping the localization dynamics. Fig. 3(c) depicts in a 3D plot the plateau width as a function of the collision rate r_c and the disorder range constant h , while varying the shape parameter ν and the anisotropy Δ , as depicted in the legend.

Overall, our results reveal that delocalization is facilitated by conditions that minimize the stabilizing effects of disorder and anisotropy. Low disorder levels ($h \ll 10$) and weak anisotropy allow noise-induced scattering to overcome any tendency toward localization, especially when combined with a higher collision rate ($1 \leq r_c \leq 10$), which disrupts coherent trapping mechanisms. Furthermore, lower values of the shape parameter ν , corresponding to temporally heterogeneous noise, contribute to more dynamic and irregular scattering events, also promoting delocalization. In contrast, higher levels of disorder ($h \geq 10$) and anisotropy, coupled with lower collision rates ($r_c \ll 1$), result in a pronounced localization. In this regime, disorder-induced traps dominate the dynamics, leading to extended plateaus where the system remains effectively localized over long timescales. We observe that the length of these plateaus scales inversely with the collision rate ($\sim 1/r_c$), consistently with the one excitation case: indeed low collision frequencies allow the system to persist in localized configurations for extended periods before noise-induced delocalization sets in.

These outcomes can be visualized also in the behavior of the complete delocalization time τ , displayed in a 3D plot Fig. 3(d) again vs disorder range h and collision rate r_c , and for different values of time-homogeneous

shape parameters ν and anisotropy Δ as in the legend. We identify four regimes, labeled with (1)-(4). (1) refers to low disorder range $h \leq 1$ with the highest shape parameter $\nu = 100$ and two values of anisotropy regimes in the collision-rate range $0.1 \leq r_c \leq 1$. Additionally, this regime extends to any disorder range when the shape parameter is high, considering the same anisotropy values in the high collision-rate range $1 \leq r_c \leq 10$. This behavior closely resembles the case without disorder ([16]) in which the complete delocalization of the excitation occurs at finite time (here, $tJ \ll 30$). (2) refers to intermediate disorder range $h = 5$ and varying collision rate r_c , time homogeneity ν , and anisotropy Δ . In this case, the complete delocalization time is $\tau < 30$. (3) refers to intermediate to large disorder bandwidth $1 < h < 10$ and the other parameters varying as in the legend. This regime is characterized by complete delocalization occurring at time $\tau \sim 30$. In particular, we see that the case with $h = 5$ and the two excitations initially injected next to each other, correspond to the formation of plateaus even with small values of disorder, thus a longer τ . Finally, (4) refers to high disorder with $h = 10$, high collision time homogeneity $\nu = 100$, two different anisotropies and collision rates $0.1 \leq r_c \leq 0.5$. Here, we see the longest τ with the formation of the longest plateaus. We conclude that delocalization is facilitated by low levels of disorder, anisotropy, and time homogeneity, along with a higher collision rate ($1 \leq r_c \leq 5$). Instead, higher levels of disorder and anisotropy, coupled with a lower collision rate, lead to more localized behaviour, with the size of the plateaus scaling as $1/r_c$. Using the plane $r_c = h$ as a reference, we observe that for $r_c < h$, the complete delocalization time remains high, while for $r_c > h$, τ is significantly reduced. This behavior resembles the case without disorder, where the complete delocalization time was indeed limited to $\tau \leq 5$.

2. The full picture

We are now ready to get the full picture, extending our investigation to explore the more general case of multiple excitations within the disordered and noisy spin chain.

To this aim, we shrink our spin chain to $N = 8$ and inject $N_{exc} = 4$ into the system, starting all next to each other to take into account the case where anisotropy plays a role. As we learned from Sec. III B 1 indeed, we restrict the parameter range to the most significant behavior. To sum up, this is for space-homogeneous (e.g. $\nu = 100$) collisions happening at low rates ($0.1 \leq r_c \leq 5$), high disorder range bandwidth (e.g. $h = 10$) and anisotropy as large as $\Delta = 2.5$.

We display in Fig. 4(a) the time evolution of the Inverse Ergodicity Ratio (IER) up to enough long time $tJ = 1000$, to let the system evolve and potentially reach a delocalized state. We see that for low collision rates ($r_c \ll 1$) combined with time-homogeneous collisions, ($\nu \gg 1$), the system is localized over a significant portion

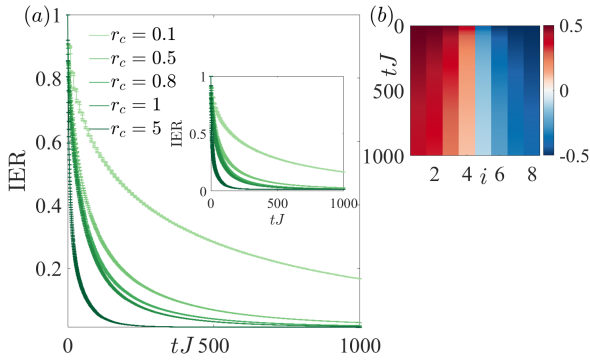


FIG. 4. Case of multiple excitations. Inverse Ergodicity Ratio (IER) (a) and color plot of the magnetization (b) for a spin chain of $N = 8$ sites and $N_{exc} = 4$ excitations starting in the middle sites, time-homogeneous collisions $\nu = 100$, with high disorder range width $h = 10$ and anisotropy strength $\Delta = 2.5$. (a) IER vs time tJ for different collision rates r_c in the interesting regime as in the legend. (b) Spread of magnetization over time tJ and sites i in the interesting regime of low collision rates, here e.g. with $r_c = 0.1$. We can overall see that low collision rates ($r_c \ll 1$) combined with time-homogeneous collisions ($\nu = 100$) lead the system to remain localized for a significant time, prolonged also by the presence of anisotropy and high disorder. Only at very long times the IER approaches its asymptotic value, signaling full delocalization. The simulations were performed with $M = 250$ trajectories and $dt = 0.02$. Final time is $tJ = 1000$.

of the evolution, especially in the presence of anisotropy and high disorder ($h \geq 10$). In such conditions, the interplay of disorder, anisotropy, and noise stabilizes localized states delaying the onset of delocalization as it is zoomed in the inset. In this case, the height of the plateaus is shorter compared to the case of one and two excitations and complete delocalization is more difficult to reach. Thus, only at very late times does the IER approach its asymptotic value, indicating that the system has completely delocalized.

To gain insight on the underlying spatial behavior, we look in Fig. 4(b) at the spread of magnetization over time, displayed as a color plot. We see that for low collision rates and high time-homogeneous collisions, the magnetization piles up for extended periods in specific regions of the spin chain, highlighting the system's localized nature. Anisotropy and disorder favor the pinning of excitations to certain sites. As time progresses, however, collisions eventually disrupt these pinned configurations, leading to gradual spread of magnetization across the chain. Delocalization is however significantly delayed under these conditions, requiring long timescales for the system to be fully delocalized.

C. Entanglement Entropy

To complement the studies based on local observables, in this section we analyze the behavior of entanglement as

a measure for thermalization dynamics in our spin chain. We focus on the case of two excitations injected into the system next to each other, that is the most interesting situation found in previous sections, where disorder, noise and coupling between spins significantly affected the delocalization behavior. We limit to two excitations for computational ease, having now clear what does change from two to more. Finally, we again zoom the parameters in the interesting range emerged in Sec. IIIB 1, that allows the emergence of plateaus and non-continuous temporal profiles of transport: this is low collision rates, e.g. with $r_c = 0.1$, large disorder range e.g. with $h = 10$ and important anisotropy e.g. with $\Delta = 2.5$. Finally, we now want to check the dependence on the noise space-homogeneity by letting the shape parameter ν vary from absence of noise ($\nu = 0$), heterogeneous collisions over time ($\nu \leq 1$) and time-homogeneous collisions ($\nu = 100$).

We then evaluate the Von Neumann entropy of the corresponding reduced density and present in Fig. 5 the time evolution of the entanglement entropy $S_{vN}(t)$ in log scale.

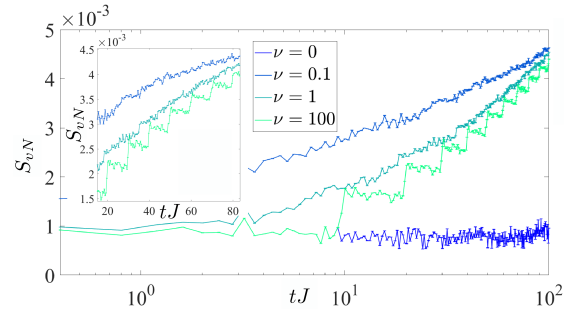


FIG. 5. Entanglement Entropy and dependence on noise space heterogeneity. S_{vN} vs time tJ in a log scale for different levels of collision-time homogeneity ν and fixed low collision rate $r_c = 0.1$, large disorder range $h = 10$ and anisotropy $\Delta = 2.5$ in the interesting plateaus regime, for a disordered spin chain of $N = 20$ sites and two injected excitations starting next to each other. Inset: same in the main figure, but in linear scale. The plot shows the mean S_{vN} over 25 of the total $M = 250$ trajectories.

In general, we expect that the low density of excitations limits the number of degrees of freedom available for generating entanglement: fewer interacting particles results in less correlations. Furthermore, we have moderate transport of information due to the presence of disorder, anisotropy and noise, which limits the spread of quantum correlations throughout the system. In the absence of noise $\nu = 0$, we observe in Fig. 5 a flat line over time, apart from some fluctuations. In fact, without noise driving perturbations that can diffuse correlations over the spin chain, the system persists in a coherent and localized state dominated only by the effects of disorder and anisotropy. For time-heterogeneous noise (low values of ν) the behavior of the entanglement entropy $S_{vN}(t)$ is logarithmic, with a slow growth consistent with the breaking of a MBL-like regime with diffusive trans-

port. Even with increasing collision time-homogeneous stroboscopic noise ($\nu = 100$), we observe the ability to also disrupt localization with the formation of plateaus. While delocalization is slower, we can tailor its rate by modifying the timescales of the plateaus as discussed in the previous sections. These plateaus are clearly visible in the inset picture in Fig. 5, in linear timescale in a reduced time range.

IV. DISCUSSION

In this study, we analyze how coherent and dissipative couplings can manipulate the transport properties and thermalization of a noisy, disordered XXZ spin chain using stochastic collisional noise to simulate the interactions with its environment. We identify relevant regimes in the rich landscape determined by the interplay between disorder, anisotropy, and collisional noise to shape the localization/delocalization transitions and the specific transport rates.

From the simplest one excitation case, see Sec. III A, we found that disorder tends to suppress transport through interference, which competes with collisional noise while the latter introduces dephasing, thus facilitating delocalization, instead. One first relevant message emerging from our study is that among these competing mechanisms, low collision rates ($r_c \ll 1$) favor the occurrence of localized regions in the form of Inverse Participation Ratio (IPR) plateaus in time windows where collisions are absent. Interestingly, the length and rate of these plateaus depend directly on noise parameters with a universal scaling, allowing to systematically tailor sequences of transport and localization that can be applied for example to stroboscopic protocols in quantum technologies. At higher collision rates ($r_c \geq 1$) instead, frequent collisional events completely disrupt localization, driving the system toward a diffusive regime characterized by smooth evolution of IPR over time, even for moderate levels of disorder range.

From the case of several excitations, see Sec. III B and Appendix B, we learn that additional features emerge due to interactions among excitations. In particular, more localized regions in the form of plateaus appear even for the tiniest levels of disorder range.

However, we still find that increasing collision rates ($r_c > 1$) disrupt localized states, promoting transport. We demonstrate the role of noise in overcoming pinning effects, down to complete delocalization in a short time τ , similar to what we found in the absence of disorder [16], where the complete delocalization times did not exceed $tJ = 5$.

In addition, we also find regimes of tunable transport and the presence of plateaus, in fact even at higher densities. In regimes with low collision rates, high shape parameter, and high disorder, entanglement entropy exhibits slow logarithmic growth, suggesting many-body localization behavior. This is consistent with the presence

of localized states that prevent rapid spread of information. Instead, for collisions heterogeneous in time, entanglement entropy more rapidly grows. Thus, homogeneous noise leads to smoother entropy dynamics.

Our analysis is of relevance for quantum technologies applications. For instance, in quantum circuits, where the efficiency of information flow directly impacts computational performance, optimizing transport is fundamental [47]. In addition, energy devices like quantum batteries and quantum heat engines could benefit from noise-engineering in order to enhance their performance in terms of efficiency and stability [23, 24]. Also, the precise manipulation of spin transport in systems such as NV centers in diamond has already enabled ultra-sensitive magnetic field measurements for quantum sensors and processors [48, 49]. Furthermore, understanding how localization-delocalization transitions arise in the presence of noise could help designing novel materials with tailored transport properties [50].

Noise-disorder engineering could be used to optimize energy transport in artificial photosynthetic complexes which could use controlled noise to enhance excitonic energy transfer, mimicking the noise-assisted transport observed in natural photosynthesis. In addition, in biological systems, where energy transfer is influenced by disorder and environmental fluctuations, tailoring noise properties at microscopic level could help to balance localization and delocalization effects, aiming at maximizing efficiency. This offers means to control energy flow in quantum networks, by tuning the connectivity and interaction strength between nodes. Along these lines, the development of programmable quantum devices could be facilitated where energy or quantum information is routed dynamically.

ACKNOWLEDGMENTS

The authors would like to thank A. Daley, G. M. Ciccini, M. C. Morrone, L. Guidi, C. Ceccanti, M. Landi and C.V. Stanzione for inspiring and useful discussions. V.S. and M.L.C. acknowledge support from the National Centre on HPC, Big Data and Quantum Computing - SPOKE 10 (Quantum Computing) and received funding from the European Union Next-GenerationEU - National Recovery and Resilience Plan (NRRP) – MISSION 4 COMPONENT 2, INVESTMENT N. 1.4 – CUP N. I53C22000690001. J.Y.M. and M.L.C. were supported by the European Social Fund REACT EU through the Italian national program PON 2014-2020, DM MUR 1062/2021. M.L.C. also acknowledges support from the project PRA2022202398 “IMAGINATION”.

Appendix A: Appendix A. Imbalance

In addition to IPR and IER, in the presence of disorder, the imbalance $\mathcal{I}(t)$ provides a descriptive figure of

merit of the system's relaxation dynamics. Indeed, we can write this figure of merit as:

$$I = n_e - \tilde{n}_o, \quad (\text{A1})$$

where $\tilde{n}_o = n_o/N - 1$, N is the number of sites and $n_e(n_o)$ is the density of even (odd) particles.

This definition incorporates the requirement that at time $t = 0$ the excitations are only present on site(s) n_e and imbalance $I = 1$. After letting the system evolve, the excitation will spread through the system to a certain degree depending on the system parameters. In a delocalized regime we have $n_e = 1/M$ and $n_o \sim 1/M$, leading to $I = 0$.

In Fig. 6, we analyze the time evolution of the imbalance $\mathcal{I}(t)$ for a disordered spin chain with $N = 41$ sites, one excitation starting in the middle of the chain and shape parameter $\nu = 100$. In particular, Fig. 6(a) shows how the Imbalance behavior varies over time for different collision rates while Fig. 6(b) shows how it varies for different disorder range constants at fixed $r_c = 1$. The imbalance $\mathcal{I}(t)$ quantifies the difference in population between the initially occupied and unoccupied regions of the chain, providing insight into the dynamics of the localization and delocalization of the system. For low collision rates ($r_c \ll 1$), the imbalance decays very slowly over time, reflecting strong localization induced by the combined effects of disorder and anisotropy.

As the collision rate increases ($r_c \sim 1$), noise events become more frequent, leading to a faster decay of $\mathcal{I}(t)$. This behavior is indicative of an improved delocalization, where excitation spreads more uniformly across the chain, erasing the initial population imbalance. The results highlight the critical role of collision rates in modulating transport properties: low rates stabilize localized states, while higher rates facilitate noise-assisted transport.

Appendix B: Appendix B. Two excitations next to each other

Here, we show additional results for the case of two excitations injected into the disordered spin chain. In particular, we present here what happens when anisotropy plays a more fundamental role in the dynamics of the system, by analyzing the Inverse Ergodicity Ratio (IER) under varying disorder regimes and excitation configurations. For excitations starting next to each other (Fig. 7(b)), anisotropy amplifies the formation of plateaus in the IER, even for low disorder levels.

In contrast, when the excitations are initially separated (Fig. 7(a)), the effects of anisotropy are subdominant, with the dynamics primarily governed by disorder and noise. These results reinforce the particular interplay between noise, disorder, and anisotropy in modulating transport properties, offering further insights into the mechanisms driving localization and delocalization transitions. The plots are for a spin chain of $N = 20$ sites,

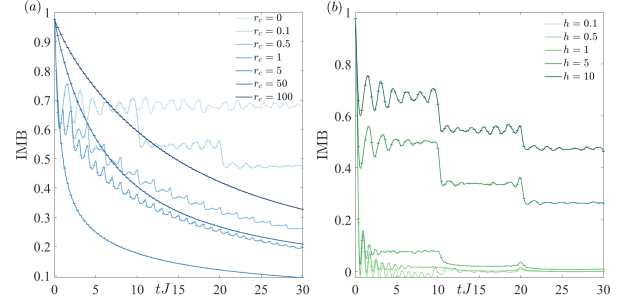


FIG. 6. Imbalance for the One excitation case. (a) Imbalance for a spin chain of $N = 41$ sites and $N_{exc} = 1$ excitations starting in the middle of the chain, shape parameter $\nu = 100$, disorder range constant $h = 10$ and interaction strength $\Delta = 0$ for different collision rates. Final time is $tJ = 30$. (b) Imbalance versus time for a spin chain of $N = 41$ sites, one excitation, different disorder range constants at fixed collision rate $r_c = 0.1$, shape parameter $\nu = 100$ and anisotropy $\Delta = 0$. The simulations were performed with $M = 500$ trajectories and $dt = 0.02$.

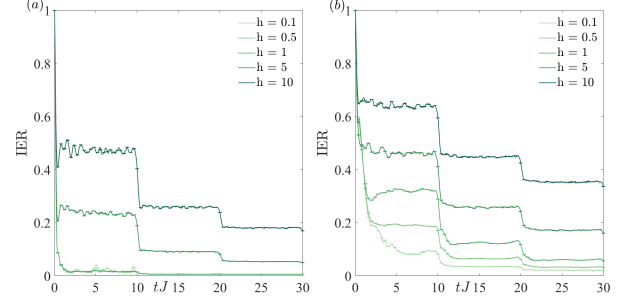


FIG. 7. Two excitations case. Inverse Ergodicity ratio (IER) for a spin chain of $N = 20$ sites and final time of simulations $tJ = 30$. (a) IER vs time tJ for different disorder range constants at fixed $r_c = 0.1$, $\nu = 100$, $\Delta = 2.5$ for two excitations starting initially separated by two spins and (b) two excitations starting next to each other. The simulations were performed with $M = 250$ trajectories and $dt = 0.02$.

at fixed $r_c = 0.1$, $\nu = 100$, $\Delta = 2.5$, varying the disorder range constants between 0.1 (low disorder) and 10 (high disorder).

- [2] D. K. Ferry, J. Weinbub, M. Nedjalkov, and S. Selberherr, A review of quantum transport in field-effect transistors, *Semiconductor Science and Technology* **37**, 043001 (2022).
- [3] M. e. A. Brahlek, Hidden transport phenomena in an ultraclean correlated metal, *Nature Communications* **15**, 5304 (2024).
- [4] J. Sebolt, M. Yu, M. Sarker, K. Lee, C. Eom, A. Sinitskii, P. Irvin, and J. Levy, Transport measurements to probe electronic states of semiconducting and metallic graphene nanoribbons, *Bulletin of the American Physical Society* (2024), d11.00004.
- [5] S. Wili, T. Esslinger, and K. Viebahn, An accordion superlattice for controlling atom separation in optical potentials, *New Journal of Physics* **25**, 033037 (2023).
- [6] M. Huang, P. Fabritius, J. Mohan, M. Talebi, S. Wili, and T. Esslinger, Limited thermal and spin transport in a dissipative superfluid junction, *arXiv preprint arXiv:2412.08525* 10.48550/arXiv.2412.08525 (2024), submitted, 12 pages, 7 figures.
- [7] M. Roy, J. J. Britto, R. Hill, and V. Onofre, Simulating open quantum systems using noise models and nisy devices with error mitigation, *arXiv preprint arXiv:2401.06535* (2024).
- [8] M. B. Plenio and S. F. Huelga, Dephasing-assisted transport: quantum networks and biomolecules, *New Journal of Physics* **10**, 113019 (2008).
- [9] D. Chisholm, G. García-Pérez, M. Rossi, G. Palma, and S. Maniscalco, Stochastic collision model approach to transport phenomena in quantum networks, *New Journal of Physics* **23**, 033031 (2017).
- [10] J. Yago Malo, G. M. Cicchini, M. C. Morrone, and M. L. Chiofalo, Quantum spin models for numerosity perception, *PLOS ONE* **18**, 1 (2023).
- [11] A. Khrennikov, Order stability via fröhlich condensation in bio, eco, and social systems: The quantum-like approach, *Biosystems* **212** (2022).
- [12] I. De Vega and D. Alonso, Dynamics of non-markovian open quantum systems, *Review of Modern Physics* **89** (2017).
- [13] H. Wiseman and G. Milburn, *Quantum Measurement and Control* (2nd ed.; Cambridge University Press, Cambridge, 2010) pp. 148–215.
- [14] H. Breuer and F. Petruccione, *The Theory of Open Quantum Systems* (2nd ed.; Oxford University Press, Oxford, 2002) pp. 390–498.
- [15] C. Gardiner and P. Zoller, *Quantum Noise* (1st ed.; Springer, Berlin, 2005) pp. 212–243.
- [16] A. Civolani, V. Stanzione, M. Chiofalo, and J. Yago Malo, Engineering transport via collisional noise: A toolbox for biology systems, *Entropy* (2024).
- [17] A. Olaya-Castro, C. F. Lee, F. Fassioli Olsen, and N. F. Johnson, Efficiency of energy transfer in a light-harvesting system under quantum coherence, *Phys. Rev. B* **78**, 085115 (2008).
- [18] N. Pathania, R. Meena, and S. Banerjee, Dynamics of quantum coherence and non-classical correlations in open quantum system coupled to a squeezed thermal bath, *arXiv preprint arXiv:2412.14913* (2024).
- [19] E. Dohner, H. Terletska, and H. F. Fotso, Thermalization of a disordered interacting system under an interaction quench, *Physical Review B* **108**, 144202 (2023).
- [20] C. Guan and X. Guan, A brief introduction to anderson localization, <https://api.semanticscholar.org> (2019), accessed from Semantic Scholar.
- [21] R. Nandkishore and D. Huse, Many-body localization and thermalization in quantum statistical mechanics, *Annual Review of Condensed Matter Physics* **6**, 15 (2015).
- [22] S. Bera, H. Schomerus, F. Heidrich-Meisner, and J. Bardarson, Many-body localization characterized from a one-particle perspective, *Physical Review B* **115**, 046603 (2015).
- [23] M. Carrega, A. Crescente, D. Ferraro, and M. Sassetti, Dissipative dynamics of an open quantum battery, *New Journal of Physics* **22**, 083085 (2020).
- [24] F. Mayo and A. Roncaglia, Collective effects and quantum coherence in dissipative charging of quantum batteries, *Physical Review A* **105** (2022).
- [25] J. e. A. Nokkala, Title to be filled (example: Quantum dynamics in complex networks), *Journal of Physics A: Mathematical and Theoretical* **57**, 233001 (2024).
- [26] E. Levi, M. Heyl, I. Lesanovsky, and J. P. Garrahan, Robustness of many-body localization in the presence of dissipation, *Physical Review Letters* **116**, 237203 (2016).
- [27] a. A. Caruso, F., Highly efficient energy excitation transfer in light-harvesting complexes: The fundamental role of noise-assisted transport, *J. Chem. Phys.* **131** (2009).
- [28] S. Huelga and M. Plenio, Vibrations, quanta and biology, *Contemporary Physics* **54**, 181 (2013).
- [29] T. Prosen and B. Buca, Connected correlations, fluctuations and current of magnetization in the steady state of boundary driven xxz spin chains, *Journal of Statistical Mechanics: Theory and Experiment* (2015).
- [30] T. Prosen and B. Buca, Integrable non-equilibrium steady state density operators for boundary driven xxz spin chains: observables and full counting statistics, *arXiv:1501.06156* (2015).
- [31] M. V. Rakov, M. Weyrauch, and B. Braierr-Orrs, Symmetries and entanglement in the one-dimensional spin-1/2 xxz model, *Physical Review B* **93** (2016).
- [32] A. J. McRoberts and R. Moessner, Ballistic conductance with and without disorder in a boundary-driven xxz spin chain, *arXiv preprint arXiv:2407.13816* 10.48550/arXiv.2407.13816 (2024), 14 pages, 10 figures.
- [33] F. Franchini, *An introduction to integrable techniques for one-dimensional quantum systems*, 1st ed. (Springer, Berlin, 2017) pp. 71–92.
- [34] T. Prosen, Open xxz spin chain: Nonequilibrium steady state and a strict bound on ballistic transport, *Phys. Rev. Lett.* **106**, 217206 (2011).
- [35] F. Gallina, M. Bruschi, and B. Fresch, Strategies to simulate dephasing-assisted quantum transport on digital quantum computers, *New J. Phys.* **24** (2022).
- [36] J. a. A. Cao, Quantum biology revisited, *Science Advances* **6**, eaaz4888 (2020).
- [37] N. Yannaros, Weibull renewal processes, *Ann. Inst. Statist. Math* **46**, 641 (1994).
- [38] G. García-Pérez, D. Chisholm, M. Rossi, G. Palma, and S. Maniscalco, Decoherence without entanglement and quantum darwinism, *Physical Review Research* **2**, 012061 (2020).
- [39] M. Rossi, C. Benedetti, M. Borrelli, S. Maniscalco, and M. Paris, Continuous-time quantum walks on spatially correlated noisy lattices, *Physical Review A* **96** (2017).
- [40] J. Deutsch, Eigenstate thermalization hypothesis, *Reports on Progress in Physics* **81**, 082001 (2018).
- [41] E. van Nieuwenburg, J. Yago Malo, A. Daley, and M. Fischer, Dynamics of many-body localization in the pres-

- ence of particle loss, *Quantum Science and Technology* **3**, 01LT02 (2018).
- [42] A. Elben, B. Vermersch, C. F. Roos, and P. Zoller, Statistical correlations between locally randomized measurements: A toolbox for probing entanglement in many-body quantum states, *Phys. Rev. A* **99**, 052323 (2019).
 - [43] R. Islam, R. Ma, and P. e. A. Preiss, Measuring entanglement entropy in a quantum many-body system., *Nature* **528**, 77–83 (2015).
 - [44] M. C. Bañuls, D. A. Huse, and J. I. Cirac, Entanglement and its relation to energy variance for local one-dimensional hamiltonians, *Phys. Rev. B* **101**, 144305 (2020).
 - [45] M. C. Bañuls, N. Y. Yao, S. Choi, M. D. Lukin, and J. I. Cirac, Dynamics of quantum information in many-body localized systems, *Phys. Rev. B* **96**, 174201 (2017).
 - [46] M. Nielsen and I. Chuang, *Quantum Computation and Quantum Information* (Cambridge University Press, 2000).
 - [47] M. Ahsan, S. A. Z. Naqvi, and H. Anwer, Quantum circuit engineering for correcting coherent noise, *Phys. Rev. A* **105**, 022428 (2022).
 - [48] F. Jelezko and P. Neumann, Quantum transport and the role of noise in quantum sensing, *Nature Materials* **11**, 10 (2012).
 - [49] L. M. Oberg, E. Huang, P. M. Reddy, A. Alkauskas, A. D. Greentree, J. H. Cole, N. B. Manson, C. A. Meriles, and M. W. Doherty, Spin coherent quantum transport of electrons between defects in diamond, *Nanophotonics* **8**, 1657 (2019).
 - [50] G. Badawy and E. P. A. M. Bakkers, Electronic transport and quantum phenomena in nanowires, *Chemical Reviews* **124**, 2419 (2024).